



An expression for the angle of repose of dry cohesive granular materials on Earth and in planetary environments

Filip Elekes^{a,1} and Eric J. R. Parteli^{b,1}

^aInstitute for Geophysics and Meteorology, University of Cologne, 50969 Cologne, Germany; and ^bFaculty of Physics, University of Duisburg-Essen, 47057 Duisburg, Germany

Edited by Risto Nieminen, Department of Applied Physics, Aalto University, Aalto, Finland, and approved August 6, 2021 (received for review April 27, 2021)

The angle of repose—i.e., the angle θ_r between the sloping side of a heap of particles and the horizontal—provides one of the most important observables characterizing the packing and flowability of a granular material. However, this angle is determined by still poorly understood particle-scale processes, as the interactions between particles in the heap cause resistance to roll and slide under the action of gravity. A theoretical expression that predicts θ_r as a function of particle size and gravity would have impact in the engineering, environmental, and planetary sciences. Here we present such an expression, which we have derived from particle-based numerical simulations that account for both sliding and rolling resistance, as well as for nonbonded attractive particle–particle interactions (van der Waals). Our expression is simple and reproduces the angle of repose of experimental conical heaps as a function of particle size, as well as θ_r obtained from our simulations with gravity from 0.06 to 100 times that of Earth. Furthermore, we find that heaps undergo a transition from conical to irregular shape when the cohesive to gravitational force ratio exceeds a critical value, thus providing a proxy for particle-scale interactions from heap morphology.

granular materials | angle of repose | dry cohesive powders | planetary geomorphology | discrete-element method

One of the most fundamental observables used to characterize the mechanical properties of a granular material, such as sand, pebbles, dust aerosols, and industrial powders, is the angle that a heap of particles makes with the horizontal—the angle of repose, θ_r . This angle is affected by particle size, because attractive particle interaction forces due to surface intermolecular and interatomic interactions become the more relevant compared to gravity and contact forces the smaller the particles are. For instance, heaps of millimeter-sized glass beads poured from a hopper display an angle of repose of about 20° to 25° (1), while the angle of repose of powders of the same material exceeds 50° (2).

However, there is no model that reliably predicts the dependence of the angle of repose of a granular material on the particle size, notwithstanding much effort made in previous work (3–6). Such a model would have the potential to substantially improve the design and control of various technological processes involving particulate systems, including in additive manufacturing technologies, in the food and pharmaceutical industry, and in the agricultural sector. Moreover, the capability of quantitatively predicting the angle of repose as a function of particle size has promising applications in the space and planetary sciences, in particular owing to increasing concern about the mechanics of granular materials in reduced-gravity experiments and extraterrestrial environments (7–9).

The derivation of an analytical expression for the angle of repose from a theoretical treatment is challenging because θ_r is dictated by still poorly understood dynamics of interparticle interactions in response to gravitational stresses. These interac-

tions are mainly due to frictional contact forces and attractive surface potentials, which enhance the cohesive behavior of the granular heap with decreasing particle size. It is uncertain how to predict the dynamics of particle–particle contacts within the granular heap, as well as the resistance to grain sliding and rolling along the heap surface.

Therefore, here we model the angle of repose by means of particle-based numerical simulations using the discrete-element method (DEM), which consists of solving Newton’s equation of motion for every particle in the system by explicitly modeling all main relevant forces acting on the particles. Using such simulations, we compute the angle of repose θ_r of spherical glass particles over the entire broad range of particle size from the micrometer to the decameter scale. As discussed in the subsequent sections, our numerical predictions for θ_r under Earth’s gravity match quantitatively a comprehensive set of experimental observations of this angle over the entire range of particle sizes investigated. Furthermore, we derive a physically based analytical expression that reproduces our DEM predictions for the angle of repose over three orders of magnitude in gravity, from Pluto conditions ($\approx 6\%$ of Earth’s gravity) up to 100 times Earth’s gravity.

In the next section we describe our numerical simulations, whereupon we present and discuss our results, the comparison of our numerical predictions with experimental observations, and our analytical model for the angle of repose. Furthermore, we show that our model is consistent with previous observations of the angle of repose in various extraterrestrial gravity conditions.

Significance

The angle between the sloping side of a heap of particles and the horizontal, called angle of repose, is often used to characterize the flowability of granular materials on Earth and planetary environments, such as sand, dust aerosols, and powders. In planetary research, this angle provides an excellent proxy for particle size. The smaller the particle is, the larger the effect of attractive forces between atoms and molecules on the surface of the particles relative to particle weight, the less flowable the material, and the steeper, thus, the angle of repose. We present a model that accurately predicts the angle of repose as a function of particle size, both on Earth and under extraterrestrial gravity.

Author contributions: F.E. and E.J.R.P. designed research; F.E. and E.J.R.P. performed research; F.E. and E.J.R.P. analyzed data; E.J.R.P. wrote the paper; F.E. performed the numerical simulations; and E.J.R.P. developed the analytical model for the angle of repose.

The authors declare no competing interest.

This article is a PNAS Direct Submission.

This open access article is distributed under [Creative Commons Attribution-NonCommercial-NoDerivatives License 4.0 \(CC BY-NC-ND\)](https://creativecommons.org/licenses/by-nc-nd/4.0/).

¹To whom correspondence may be addressed. Email: f.elekes@uni-koeln.de or eric.parteli@uni-due.de.

Published September 13, 2021.

To conclude this article, we briefly discuss possible implications of our study for future research and present an outlook for model improvements.

Numerical Experiments

The DEM, which we apply in our numerical simulations, was introduced by Cundall and Strack (10) and has been steadily refined in the course of recent decades to incorporate improved particle–particle interaction models (11–15). Our DEM, revised in *Materials and Methods*, accounts for all main relevant forces acting on the particles, i.e., gravity, frictional contact forces, and attractive van der Waals forces, and has proved to reproduce quantitatively the solid fraction and the packing structure of powders constituted of different materials (15, 16).

One widely employed method to generate a granular heap is the fixed funnel method, where the granular material is poured through a funnel or orifice onto a rough surface. In another method, a hollow cylinder, placed atop the surface, is filled with the particulate material and then pulled off of the base at low velocity, to allow the particles to flow down through the cylinder’s bottom end (17). However, it is difficult to control heap formation using these methods in numerical simulations of strongly cohesive particles, given that such simulations involve a sensibly small number of particles, thus increasing the tendency to form a clump encompassing a large fraction of the particles in the system. Therefore, we employ a different method that can be regarded as a combination of the fixed funnel and the hollow cylinder method.

The heap is formed by pouring particles onto a frictional, square horizontal plate, which has sides $40d$ and constitutes the bottom wall of the simulation domain—a rectangular box of horizontal dimensions $40d \times 40d$ and height $30d$. The particle insertion region has a square cross-section of side length $4.4d$, is centered around the vertical symmetry axis of the simulation domain, and extends from the top of the simulation domain down to a height of $20d$ above the bottom plate. At time $t = 0$, particles are placed at random positions throughout the inner volume of the insertion region, thereby producing a packing of solid fraction $\approx 20\%$. Thereafter, the particles are released from rest.

Particle insertion is repeated at an insertion time step $\Delta t_{ins} \approx 3.5\sqrt{d/g}$, i.e., the time interval between two consecutive insertion events, with g standing for gravity. However, during the pouring process, once the height of the growing heap has exceeded $20d$, only the remaining upper free volume of the insertion region above the heap crest is used for particle insertion. Moreover, the number of poured particles is 25,000, but the pouring process is interrupted if the heap’s crest reaches the top of the simulation domain.

Open boundary conditions are applied in the horizontal directions. Therefore, the number of particles constituting the final heap can differ depending on d and g , since particles that abandon the simulation domain through its lateral borders are not replaced by new particles. The number of particles constituting the heaps produced in the present study varied between 5,000 and 14,000.

Results and Discussion

Angle of Repose Predicted from DEM Simulations. Fig. 1 displays snapshots of simulations obtained with $d = 30\ \mu\text{m}$ and $d = 1\ \text{mm}$ under terrestrial gravity conditions. To measure the angle of repose, the projection of the heap on two orthogonal planes (x and y) is computed, which yields two side-view images of the heap separated by a rotation of 90° . An image-processing algorithm is then applied to compute the upper boundary of the granular material, i.e., the heap surface, as well as the total surface area associated with the two-dimensional heap projection. Following ref. 18, we define the angle of repose as the base angle

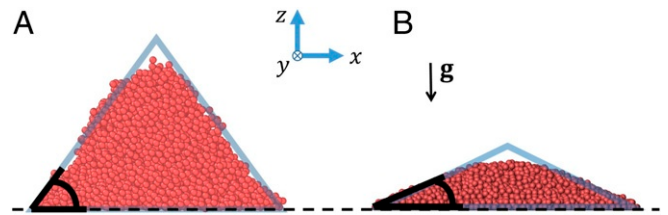


Fig. 1. Snapshots of granular heaps produced in our simulations. In *A* we see a heap constituted by particles of diameter $d = 30\ \mu\text{m}$, while particle size in *B* is $d = 1\ \text{mm}$. The span of each heap is equal to $40d$, and both heaps have been produced using terrestrial gravity.

of the isosceles triangle, which has the same surface area as the heap (Fig. 1). Therefore, two values of this angle are obtained for each heap, from which the mean θ_r and SD σ_{θ_r} are computed. We have found no considerable changes in the angle of repose by including computations of this angle from additional projections separated by smaller rotation angles (18).

Moreover, we have found that heaps formed by particles of diameter smaller than a value d_c ($\approx 50\ \mu\text{m}$ under terrestrial gravity) display a strongly irregular shape, with considerable variations in local slope throughout their surface (Fig. 1*A*). In this regime of strongly irregular heap morphology, which we call here regime I, particle avalanches are largely inhibited by the formation of large, irregular particle agglomerates along the surface of the heap. By contrast, heaps formed with particles of size $d \gtrsim d_c$ (regime II) display rather regular morphology and nearly constant slope along their surface (Fig. 1*B*).

We remark that it becomes increasingly difficult to produce heaps in our simulations as d decreases down to values smaller than d_c . In particular, we could not obtain any heap for d smaller than about 50% of d_c , since particles’ sticky behavior for such small particle sizes causes the heap to reach the upper limit of the simulation domain. The conclusions presented in our article are thus applicable to heaps in regime II, i.e., provided particles are not smaller than about d_c .

The solid squares in Fig. 2 denote the values of $\theta_r(d)$ obtained from DEM simulations under Earth’s gravity. Moreover, Fig. 2 also displays a comprehensive compilation of experimental data for the angle of repose as a function of particle size, taken from measurements of θ_r from granular heaps produced with different materials (see legend and key in Fig. 2). As we can see in Fig. 2, our numerical predictions follow remarkably well the trend of the experimental data.

Furthermore, Fig. 3*A* shows the values of θ_r obtained for different values of gravity, ranging from Pluto gravity ($g = 0.62\ \text{m/s}^2$) to 100 times Earth’s gravity. We see that the same qualitative behavior of θ_r as a function of d is found for all values of gravity investigated. Moreover, for a given particle size, a trend of increasing θ_r with decreasing gravity is observed. In the following section we present a mathematical expression that will shed light on our numerical predictions, as well as on the experimental observations of the angle of repose as a function of particle size.

A Mathematical Expression for the Angle of Repose as a Function of Gravity and Particle Size. To obtain a mathematical expression that fits our DEM predictions for θ_r as a function of particle size, we first note that the angle of repose is described via $\theta_r \approx \tan^{-1}[\mu_{\text{eff}}]$, where μ_{eff} is an effective coefficient of friction describing the maximal friction resistance of the granular material against sliding through avalanche (23). This coefficient encodes information on material properties, as well as on macroscopic characteristics related to the heap structure, such as packing fraction and surface roughness.

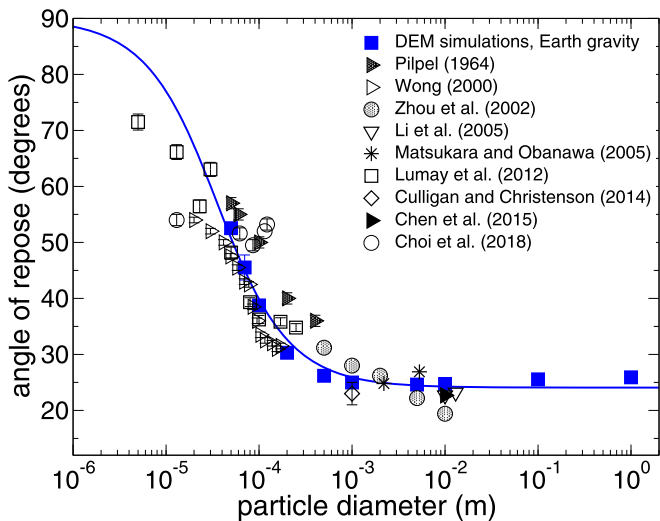


Fig. 2. Angle of repose as a function of the particle diameter. Solid blue squares indicate the predictions from our numerical simulations, performed with the parameters listed in Table 1 and using $g = 9.81 \text{ m/s}^2$. The other symbols denote experimental observations made for roughly monodisperse systems, i.e., the scenario of our DEM simulations. All shown experimental data correspond to glass beads (1, 2, 5, 19–22), except for Pilpel (3) (magnesium oxide) and Lumay et al. (18) (silicon carbide abrasives). The solid line denotes the best fit to our numerical predictions using Eq. 1, which yields $D_E \approx 87 \text{ }\mu\text{m}$, and $\mu_{\text{eff},\infty} \approx 0.447$.

However, these characteristics are affected by the nature of interparticle interaction forces. As particle size decreases, attractive particle interaction forces become increasingly more relevant compared to gravitational forces, thereby leading to an increase in the bulk porosity and affecting the dynamics of stress distribution within the heap. Experiments and DEM simulations revealed that the solid fraction of powders follows, approximately, a power-law relation with particle size (15). Taking inspiration from this insight, we approximately describe θ_r (in radians) using the expression

$$\theta_r \approx \tan^{-1} \left\{ \mu_{\text{eff},\infty} \cdot \left[1 + \frac{D}{d} \right] \right\}, \quad [1]$$

where the effective friction coefficient $\mu_{\text{eff},\infty}$ and the characteristic length-scale D must be determined from the best fit to observations of the angle of repose as a function of particle size. The best fit to our simulation data (blue solid squares in Fig. 2) using Eq. 1 gives $\mu_{\text{eff},\infty} \approx 0.447$ and $D \approx 87 \text{ }\mu\text{m}$, with coefficient of correlation $R^2 \approx 99\%$. This best fit is denoted by the solid line in Fig. 2.

Moreover, the solid lines in Fig. 3A denote the best fits to the DEM results associated with various values of g level; i.e., $\tilde{g} = g/g_{\text{Earth}}$, where $g_{\text{Earth}} = 9.81 \text{ m/s}^2$, using Eq. 1 and assuming that $\mu_{\text{eff},\infty} \approx 0.447$ is independent of gravity. The dotted line in Fig. 3A corresponds to the asymptotic value of the angle of repose, $\theta_{r,\infty} \equiv \tan^{-1}[\mu_{\text{eff},\infty}]$. Indeed, we find that the angle of repose $\theta_{r,\text{nc}}$ obtained from simulations without attractive particle interaction forces (i.e., assuming noncohesive materials) is approximately equal to $\theta_{r,\infty}$, independent of particle size (Fig. 3B). There is a small trend of increasing $\theta_{r,\text{nc}}$ with gravity—Fig. 3B suggests an increase of the order of 10% in $\theta_{r,\text{nc}}$ with an increase in \tilde{g} from 0.06 to 100—which we attribute to a slightly greater tendency of particles to interlock upon an increase in gravitational stress, but further work (not in the scope of this article) would be needed to elucidate this small effect. Fig. 3A and

B thus shows that particle size controls on θ_r are dictated mainly by cohesive particle–particle interactions.

Fig. 3C displays the values of D obtained from the best fits in Fig. 3A, as a function of the g level. As we can see from Fig. 3C, for the range of \tilde{g} considered in the present work, the characteristic length-scale D can be approximately described by the equation

$$D = \frac{D_E}{\sqrt{\tilde{g}}}, \quad [2]$$

where D_E denotes the terrestrial value of D , i.e., $87 \text{ }\mu\text{m}$. We remark that the solid red line in Fig. 3C is not fit to the simulation data (solid circles). Instead, the red line denotes Eq. 2, i.e., our conjecture that D is equal to $D_E/\sqrt{\tilde{g}}$. We have found that fitting the DEM results using the equation $D = D_0/\tilde{g}^\alpha$ leads to

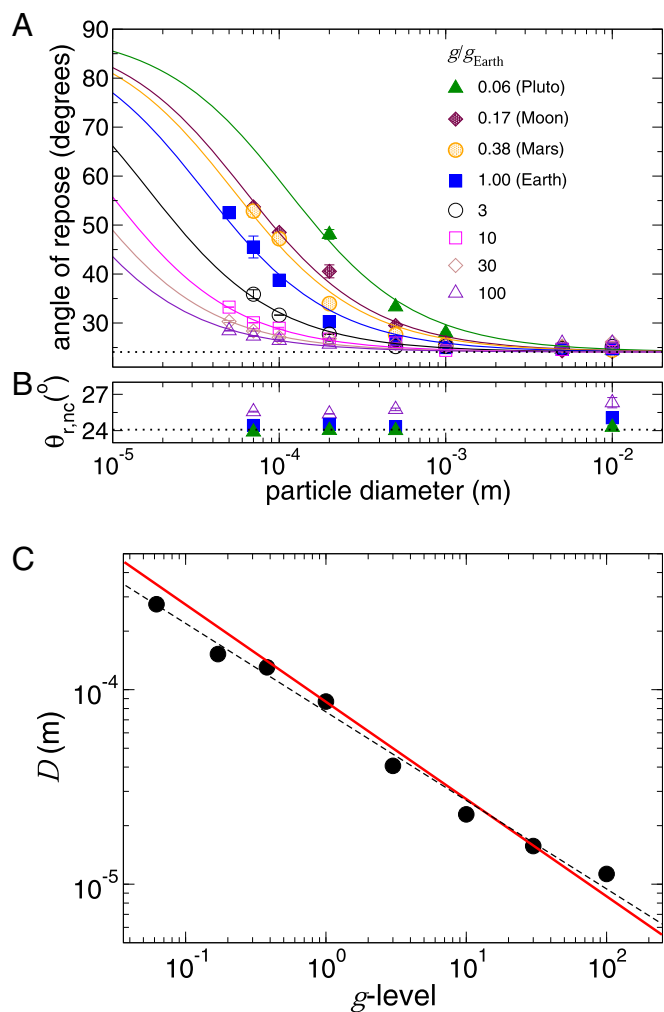


Fig. 3. Effect of gravity on the angle of repose. In A, symbols denote $\theta_r(d)$ for various g levels, ranging from gravity conditions on Pluto to 100 times Earth’s gravity. The solid lines in this plot indicate the best fits to the simulation data using Eq. 1, assuming $\mu_{\text{eff},\infty} = 0.447$. Furthermore, symbols in B denote the angle of repose $\theta_{r,\text{nc}}$ obtained from simulations without cohesive forces, while the dotted line in A and B indicates the value $\theta_{r,\infty} \equiv \tan^{-1}[\mu_{\text{eff},\infty}]$. The values of D obtained from the best fits in A are shown in C as a function of the g level. The solid line in C represents Eq. 2, using $D_E = 87 \text{ }\mu\text{m}$ as obtained from the best fit to the DEM data with Earth’s gravity (Fig. 2). Furthermore, the dashed line denotes the best fit to our numerical predictions of D as a function of \tilde{g} using $D = D_0/\tilde{g}^\alpha$, which yields $D_0 \approx 76 \text{ }\mu\text{m}$ and $\alpha \approx 0.454$ with coefficient of correlation larger than 99%.

$D_0 \approx 76 \mu\text{m}$ and $\alpha \approx 0.45$ with coefficient of correlation larger than 99% (dashed line in Fig. 3C), which provides, thus, an exponent close to 0.5 as assumed in Eq. 2.

Using Eq. 2 we can rewrite Eq. 1 as

$$\theta_r \approx \tan^{-1} \left\{ \mu_{\text{eff},\infty} \cdot \left[1 + \frac{1}{(d/D_E) \cdot \sqrt{g}} \right] \right\}, \quad [3]$$

which provides a means to estimate θ_r (in radians) for given g and d , provided D_E and $\mu_{\text{eff},\infty}$ for the granular material are known, e.g., from experiments under terrestrial gravity.

From Eq. 3, we see that, in the limit $\sqrt{g}d/D_E \rightarrow \infty$, the angle of repose asymptotically approaches the value $\theta_{r,\infty} \equiv \tan^{-1}[\mu_{\text{eff},\infty}]$, independent of gravity and particle size. For the particulate material investigated here, $\theta_{r,\infty} \approx 24^\circ$ (Figs. 2 and 3). Therefore, an approximate value for $\mu_{\text{eff},\infty}$ can be estimated from experiments using particles that are so large that cohesive effects on the angle of repose can be neglected, whereupon $\mu_{\text{eff},\infty}$ can be computed using the equation $\mu_{\text{eff},\infty} = \tan(\theta_{r,\infty})$. Subsequently, experiments under Earth's gravity using different values of d can be performed to estimate D_E from the best fit to Eq. 3.

To shed light on Eq. 3, we note that granular materials display increasing relative cohesiveness the smaller the particle size is (15). We follow refs. 24 and 25 and characterize this cohesiveness by computing the Bond number (Bo), i.e., the ratio of the maximum cohesive force acting on a particle to the gravitational force. For the system investigated here, we obtain $\text{Bo} = 12\gamma/(d^2g\rho_p)$ (using Eqs. 13 and 14), where ρ_p is the material density and γ is the surface energy density, which scales the attractive interparticle (van der Waals) force. Given this expression for the Bond number and the scaling of the angle of repose with the particle size in Eq. 3, we propose the model

$$\theta_r \approx \tan^{-1} \left\{ \mu_{\text{eff},\infty} \cdot \left[1 + \beta\sqrt{\text{Bo}} \right] \right\}, \quad [4]$$

where $\mu_{\text{eff},\infty}$ and β are empirical parameters. As shown in Fig. 4, using this model, we find an excellent data collapse of our simulation results for all values of particle size and gravity con-

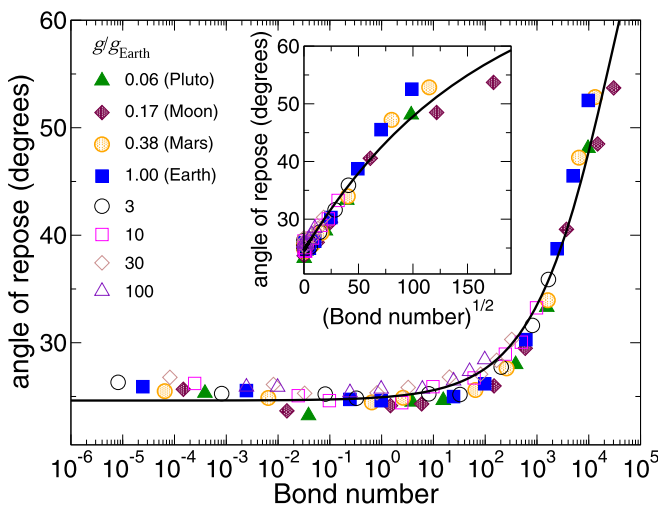


Fig. 4. Main plot: Angle of repose θ_r as a function of the Bond number. Symbols indicate predictions from numerical simulations under different g levels. Moreover, the solid line in the main plot denotes the best fit to the simulation data using Eq. 4, which yields $\mu_{\text{eff},\infty} \approx 0.458$ and $\beta \approx 0.014$ ($R^2 \approx 0.98$). The data shown in the main plot are replotted in *Inset*, which shows the angle of repose θ_r as a function of $\sqrt{\text{Bo}}$, using linear scale for both axes.

sidered, with $\mu_{\text{eff},\infty} \approx 0.458$ and $\beta \approx 0.014$. Furthermore, from the definition of Bo, Eqs. 1 and 4 lead to

$$D = \beta \sqrt{\frac{12\gamma}{\rho_p g}}, \quad [5]$$

which relates the characteristic length-scale D in Eq. 1 to the material parameters.

We note that our model is valid in the regime of regular heap morphology (regime II), i.e., when $d \gtrsim d_c$. In particular, Eq. 1 predicts $\theta_r \rightarrow 90^\circ$ when $d \rightarrow 0$, but experiments revealed a nearly constant angle of repose for particle sizes of the order of a few micrometers, i.e., in regime I of irregular heap morphology (26). Our simulations show that $D \approx 2d_c$ and that the heap morphology changes from regular (regime II) to irregular (regime I) when the Bond number exceeds approximately 10^4 , thus providing a means to approximately estimate d_c from the material properties.

We have also performed some simulations with heaps 150% larger than the ones considered in the present discussion, but we could not find a significant change in the values of θ_r . We believe that, qualitatively, even larger heaps should display the same dependence of θ_r on d observed in the experiments quoted in Fig. 2 and in the DEM simulations in this article. However, it is uncertain to which extent our model parameters should be adapted to assess the angle of repose of much larger heaps quantitatively. In particular, the dynamics of much larger systems could be affected by particle–air interactions, which must be incorporated in a future extension of our model. Furthermore, since the packing dynamics are affected by the preparation history of the packing (see the discussion in ref. 15), the pouring height and the size of the insertion region chosen for reproducing experimental conditions could exert an important control on the value of θ_r . We have indeed noticed a trend of increasing avalanche sizes by increasing the width of the particle insertion region in our simulations of larger heaps. Therefore, the quantitative behavior of θ_r for much larger heaps will constitute topic of future research.

An argument for the approximate scaling with the square root of the Bond number in Eq. 4. Our model suggests that the effective friction coefficient μ_{eff} can be written as

$$\mu_{\text{eff}} \approx \mu_{\text{eff},\infty} \cdot [1 + f], \quad [6]$$

where $\mu_{\text{eff},\infty}$ is the value of μ_{eff} disregarding the contribution from attractive particle interaction forces, encoded in the value of f . Furthermore, an approximate scaling of f with $\sqrt{\text{Bo}}$ is obtained from our simulations (Eq. 4).

To shed light on this scaling, we note that, when the local slope exceeds the angle of repose, the heap surface relaxes through avalanches, thus leading to the emergence of a surface avalanche layer—of thickness a few times d and constituted of N particles—flowing downhill atop the immobile granular bulk in the heap's interior. At the angle of repose, the downhill gravitational force on these N particles, i.e., $W = Nmg$, with m denoting the particle mass, is balanced by frictional contact forces and cohesive interactions with particles in the bulk. However, not all N particles participate in these interactions. Instead, the total cohesive force acts on a subset $N_{\text{interface}}$ of particles that are at the interface with the bulk. We propose that f scales with the quotient of this total cohesive force and W ; i.e.,

$$f \propto \frac{N_{\text{interface}} \cdot F_{\text{vdW}}}{Nmg} \propto \frac{N_{\text{interface}}}{N} \cdot \frac{1}{d^2g}, \quad [7]$$

where we used $m \propto d^3$ and $F_{\text{vdW}} \propto d$, with F_{vdW} standing for the attractive van der Waals force (Eq. 13) between a particle in

the avalanche layer and another particle in the bulk. Therefore, a scaling of f with \sqrt{Bo} , i.e., with $(d\sqrt{g})^{-1}$, is obtained if $\eta \equiv N_{\text{interface}}/N \propto d\sqrt{g}$, which must be verified through numerical simulations.

However, here we assume that η is, to first order, proportional to the packing density (ϕ) of the granular material. We think that this assumption is reasonable, because the smaller ϕ is, the more porous the granular medium and the smaller, thus, η is. By contrast, the denser the granular material is, the larger the number of particle–particle contacts, and the larger, thus, η is. To verify whether ϕ (and thus η) follows, to a certain limit, an approximate scaling with $d\sqrt{g}$, we have performed numerical experiments adapting the protocol of ref. 15 to investigate the effect of d and g on ϕ . Fig. 5 displays the results of these experiments, which are described at the end of *Materials and Methods*.

As can be seen in Fig. 5, the plot of ϕ as a function of $d\sqrt{g}$ leads to an excellent data collapse of our simulation results and reveals an asymptotic growth of the packing fraction with $d\sqrt{g}$. Specifically, in the limit of large particle sizes ($d \gtrsim 1$ mm), the granular material displays a largely noncohesive behavior, with ϕ resulting nearly independent of $d\sqrt{g}$. The dashed line in the main plot in Fig. 5 denotes the best fit using the asymptotic growth function $\phi = \phi_{\infty} \cdot \{1 - C \cdot \exp[-D_{\phi}^{-1} \cdot d\sqrt{g}]\}$, which gives $\phi_{\infty} \approx 0.57$ (the associated random loose packing fraction) (27), $C \approx 0.56$, and $D_{\phi} \approx 103 \mu\text{m}$, with correlation coefficient $R^2 \approx 0.994$. We remark that a theoretical model is needed to elucidate this scaling, as well as the behavior of ϕ as $d\sqrt{g} \rightarrow 0$. However, such a theoretical model would go beyond the scope of the present discussion, which aims rather at testing for an approximate scaling of ϕ with $d\sqrt{g}$ to a certain limit.

Indeed, a linear fit using $\phi = A + B \cdot d\sqrt{g}$ describes reasonably well the trend of the simulation results associated with the lower range of $d\sqrt{g}$ considered in the present article; i.e., $30 \leq [d\sqrt{g}]/\mu\text{m} \leq 210$, with $A \approx 0.32$, $B \approx 1.14 \text{ mm}^{-1}$, and correlation coefficient $R^2 \approx 0.947$ (Fig. 5, *Inset*). The origin of this approximate linear trend is the effect of attractive particle interaction forces—which are relevant in the aforementioned range

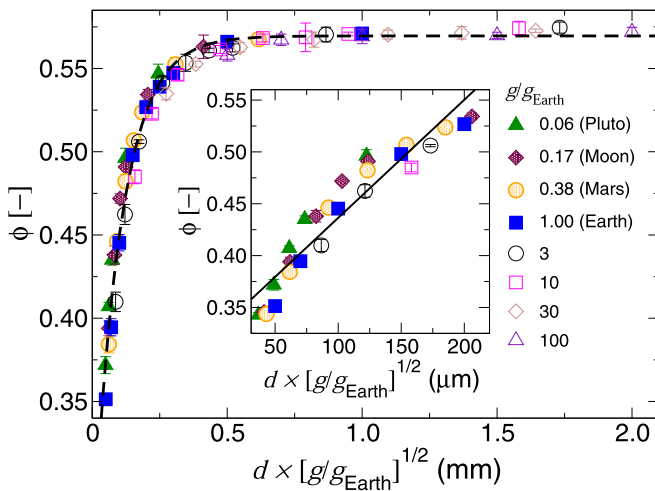


Fig. 5. Packing density ϕ as a function of $d\sqrt{g}$, with $\tilde{g} \equiv g/g_{\text{Earth}}$. The dashed line in the main plot denotes the best fit to the simulation results (symbols) using the equation $\phi = \phi_{\infty} \cdot \{1 - C \cdot \exp[-D_{\phi}^{-1} \cdot d\sqrt{g}]\}$, which yields $\phi_{\infty} \approx 0.57$, $C \approx 0.56$, and $D_{\phi} \approx 103 \mu\text{m}$, with $R^2 \approx 0.994$. Furthermore, the solid line in *Inset* denotes the best linear fit to the simulation results within the range $30 \leq d/\mu\text{m} \leq 210$, using $\phi = A + B \cdot d\sqrt{g}$, which gives $A \approx 0.32$ and $B \approx 1.14 \text{ mm}^{-1}$, with $R^2 \approx 0.947$.

of small $d\sqrt{g}$, but become negligibly small compared to particle weight when $d\sqrt{g}$ becomes sufficiently large. We thus find that the approximate linear scaling of ϕ (and, thus, of $\eta \equiv N_{\text{interface}}/N$) with $d\sqrt{g}$, within the range of small $d\sqrt{g}$, provides an argument for the approximate scaling of f with \sqrt{Bo} , owing to Eq. 7. More precisely, $f \propto \eta/[d^2g] \propto \phi/[d^2g] \propto 1/[d\sqrt{g}]$ (i.e., $f \propto \sqrt{Bo}$).

Significance of Our Model in the Light of Experimental Observations. Reduced-gravity experiments of granular heap formation (28) in the Bremen drop tower, using basalt beads of diameter $500 \mu\text{m}$, revealed a slight trend of increasing angle of repose with decreasing gravity for $0.03 \leq \tilde{g} \leq 1$. Although the experiments were performed using a Hele–Shaw cell to obtain quasi-2D heaps (28), qualitatively, the behavior of θ_r with gravity for these heaps is consistent with the prediction from our model that granular materials behave more cohesively and produce larger angles of repose under lower gravity.

Furthermore, parabolic flight experiments with slowly rotating drums, operating in the discrete avalanche regime at g levels ranging from 0.1 to 1, revealed a slight trend of increasing angle of repose θ_{start} —the slope above which the granular surface becomes unstable and starts to avalanche (29)—with decreasing gravity (30, 31). The increase of θ_{start} with decreasing g observed in ref. 30 suggests enhanced cohesive behavior of granular materials under reduced gravity (30). Microgravity experiments with rotating drums operating at g levels varying from 0.01 to 1.9 and at high rotational speeds, in the so-called continuous avalanching regime—in which the granular surface undergoes avalanche flow permanently—also revealed increasing cohesive behavior with decreasing g (32, 33). In these experiments, a scaling of the slope angle of the granular surface with $\sqrt{1/g}$ was found (32, 33). To compare, experiments in the centrifuge at g levels from 1 to 25 revealed insignificant correlation between this angle and gravity (34), as also predicted from our model.

We note that particle interaction forces can be affected by still poorly understood geochemical processes (35), while granular flows under low atmospheric pressure conditions can be further influenced by the presence of interstitial gas. Moreover, for values of Bond number smaller than unity, irregular particle geometries, inherent to natural granular systems, can cause statistical fluctuations comparable to the difference between the angles of repose predicted for spherical particles under g levels of the same order. For instance, parabolic flight experiments using Toyoura sand ($d \approx 250 \mu\text{m}$) revealed no significant dependence of the angle of repose on gravity for the range of investigated g levels (1/6 to 2) (36). We conclude, based on our results, that the angle of repose of natural sand under Martian gravity should not differ much from its terrestrial counterpart (30° to 35°), which is consistent with observations from the slope of Martian dunes at their avalanche side (37).

Characterization of average particle size of strongly polydisperse systems can be made using different parameters, such as the Sauter mean particle size d_S , i.e., the diameter of the particle that has the same volume to surface area ratio as the entire ensemble. Two comprehensive compilations of experimental datasets on θ_r as a function of d_S , presented in refs. 26 and 38, reveal the same characteristics as in Fig. 2, i.e., a noticeable, power-law-like decrease with d_S within an intermediate range of particle size, followed by slower decay in the limit of larger d_S , with θ_r asymptotically approaching a value $\theta_{r,\infty}$ between 20° and 30° that is roughly independent of particle size. We thus propose that Eq. 1 should be valid without regard of the parameter employed to characterize particle size, since the

corresponding value of D can be estimated from the best fit to $\theta_r(d)$ using Eq. 1.

We further remark that Eq. 1 should break down when d becomes much smaller than a certain value (d_c), which, for the system considered in our DEM simulations, is of the order of $50 \mu\text{m}$. Indeed, Eq. 1 predicts that $\theta_r \rightarrow 90^\circ$ as $d \rightarrow 0$. However, measurements of θ_r of strongly polydisperse dust systems (using the Sauter mean diameter d_S to characterize particle size) revealed a breakdown in the trend of increasing θ_r with decreasing particle size, when particles become sufficiently small (26). As explained by Lanzerstorfer (26), the reason for this behavior is the formation of small agglomerates of dust-sized particles, which roll down the heap slope, thus limiting the angle of repose. An upper limit for θ_r of about 55° was reported in the experiments in ref. 26.

Although further work will be required to characterize the dynamics of particle agglomerates in DEM simulations and to investigate the factors controlling the value of d_c , we note that the highest values of θ_r in most experimental datasets quoted in Fig. 2 are consistent with the upper bound reported by Lanzerstorfer (26). The only exception is the dataset of Lumay et al. (18) (open squares in Fig. 2), which displays θ_r exceeding 70° . A possible explanation for the higher θ_r values in this dataset is that the silicon carbide abrasives adopted in ref. 18 consist of a broad distribution of complex particle geometric shapes, including elongated and sharp-edged particles. DEM simulations (39) have shown that cohesive rods form packings of lower solid fraction than that of cohesive beads; i.e., complex particle shapes can enhance the cohesive behavior of granular materials. By virtue of these observations and in view of our Eqs. 4 and 7, we thus expect that elongated particles, compared to beads, produce steeper heaps, while sharp edges could further enhance friction and heap stability. The present work could be thus continued by elucidating this behavior in DEM simulations.

However, future work should now focus on deepening the understanding of our findings from a theoretical analysis of granular heap stability, which poses a long-standing and challenging research topic in the field of granular matter physics (40).

Materials and Methods

This section describes the DEM employed in our numerical simulations.

Equations of Motion. The equations for the translational and rotational motion of the i th particle in the system read

$$m\ddot{\mathbf{r}}_i = \sum_{\substack{1 \leq j \leq n \\ j \neq i}} \mathbf{F}_{ij} + m\mathbf{g} \quad [8]$$

$$I\dot{\boldsymbol{\omega}}_i = \sum_{\substack{1 \leq j \leq n \\ j \neq i}} \mathbf{M}_{ij}, \quad [9]$$

where \mathbf{r}_i and $\boldsymbol{\omega}_i$ denote the position and angular velocity of particle i , respectively; \mathbf{g} is gravity; while \mathbf{F}_{ij} and \mathbf{M}_{ij} denote the interaction force and torque, respectively, exerted by particle j on particle i . Furthermore, n is the total number of particles in the system, each particle having diameter d , density ρ_p , mass $m = \pi\rho_p d^3/6$, and moment of inertia $I = md^2/10$. In Eq. 8, \mathbf{F}_{ij} denotes the sum of the contact force \mathbf{F}_{ij}^c and the nonbonded attractive interaction force \mathbf{F}_{ij}^a exerted by particle j on particle i . These forces are modeled as discussed next.

Particle-Particle Interaction Forces. For the normal component of the contact force, $\mathbf{F}_{ij,n}^c$, viscoelastic interaction is assumed (11), while a modified Cundall-Strack model (10) is applied to compute the tangential force, $\mathbf{F}_{ij,t}^c$. The equations for $\mathbf{F}_{ij,n}^c$ and $\mathbf{F}_{ij,t}^c$ read

$$\mathbf{F}_{ij,n}^c = \min \left(0, -k_n \delta_{ij,n}^{3/2} - \frac{3}{2} A_n k_n \sqrt{\delta_{ij,n} \dot{\delta}_{ij,n}} \right) \mathbf{e}_{ij,n} \quad [10]$$

$$\mathbf{F}_{ij,t}^c = - \min \left(\mu_s |\mathbf{F}_{ij,n}^c|, \int_{\text{path}} k_t \sqrt{\delta_{ij,n}} ds + A_t \sqrt{\delta_{ij,n}} v_{ij,t} \right) \mathbf{e}_{ij,t}, \quad [11]$$

Table 1. Numerical values of parameters used in the simulations

Parameter	Symbol	Value
Young's modulus	Y	63 GPa
Poisson's ratio	ν	0.24
Particle material density	ρ_p	2,500 kg/m ³
Surface energy density	γ	0.05 J/m ²
Sliding friction coefficient	μ_s	0.5
Rolling friction coefficient	μ_r	0.05

where $\delta_{ij,n} = d - |\mathbf{r}_j - \mathbf{r}_i|$; $\mathbf{e}_{ij,n} = \frac{\mathbf{r}_j - \mathbf{r}_i}{|\mathbf{r}_j - \mathbf{r}_i|}$; \mathbf{r}_i and \mathbf{r}_j are the positions of particles i and j , respectively; $v_{ij,t} = |\mathbf{v}_{ij,t}|$, where $\mathbf{v}_{ij,t} = \mathbf{v}_{ij} - (\mathbf{v}_{ij} \cdot \mathbf{e}_{ij,n}) \cdot \mathbf{e}_{ij,n}$ denotes the relative tangential velocity at the point of contact, with $\mathbf{v}_{ij} = \dot{\mathbf{r}}_j - \dot{\mathbf{r}}_i$; and $\mathbf{e}_{ij,t} = \mathbf{v}_{ij,t}/v_{ij,t}$ is the tangential unit vector; while the contact forces in Eqs. 10 and 11 are set as zero if $\delta_{ij,n} < 0$. Furthermore, k_n and k_t are elastic parameters, which are computed from the particle Young's modulus, Y , and the Poisson's ratio, ν , through

$$k_n = \frac{2Y}{3(1-\nu^2)} \sqrt{R_{\text{eff}}}, \quad k_t = \frac{4G}{2-\nu} \sqrt{R_{\text{eff}}} \quad [12]$$

with $G = Y/(2 + 2\nu)$ denoting the shear modulus and $R_{\text{eff}} = d/4$, while A_n and A_t are dissipative parameters, μ_s is the (Coulomb) sliding friction coefficient, and the integral in Eq. 11 is performed over the relative displacement of the particles at the point of contact and over the entire contact duration (15, 41).

The dissipative parameter A_n further depends on material viscosities that are not directly available (11). Therefore, to determine A_n , we use a relation between this dissipative parameter and the coefficient of restitution for the collision of two isolated particles (42, 43) and employ the Padé approximation from ref. 44. Furthermore, following ref. 45, we choose the tangential dissipative parameter, A_t , such that the prefactors of $\dot{\delta}_{ij,n}$ and $v_{ij,t}$ in Eqs. 10 and 11, respectively, are of the same order of magnitude, thus yielding $A_t = 3A_n k_n/2$. Indeed, ref. 46 showed that this assumption leads to excellent agreement between simulation results and experimental values of particle velocity profiles in a gravity-driven shearing experiment.

Furthermore, the nonbonded attractive van der Waals interaction force between two particles in the system, labeled i and j , is given by (15, 47, 48)

$$\mathbf{F}_{ij,n}^a = \begin{cases} \frac{A_H R_{\text{eff}}}{6D_{\text{min}}^2} \mathbf{e}_{ij,n} & \text{if } \delta_{ij,n} > 0, \\ \frac{A_H R_{\text{eff}}}{6(\delta_{ij,n} - D_{\text{min}})^2} \mathbf{e}_{ij,n} & \text{if } -D_{\text{max}} \leq \delta_{ij,n} \leq 0 \\ 0, & \text{if } \delta_{ij,n} < -D_{\text{max}}, \end{cases} \quad [13]$$

where A_H is the Hamaker constant, which is computed from the surface energy density, γ , using the expression (49)

$$A_H = 24 \pi D_{\text{min}}^2 \gamma. \quad [14]$$

In Eq. 13, D_{max} is the maximal (cutoff) distance of the van der Waals interaction, which is set as $1 \mu\text{m}$ (15), while the constant D_{min} is introduced to avoid the singularity of the Hamaker equation at $\delta_{ij,n} = 0$ and accounts for the fact that particles are not perfectly smooth. We take the value $D_{\text{min}} = 1.65 \text{ \AA}$, which corresponds to the minimal distance between particles at contact (49, 50).

Torque and Rolling Friction. The total torque \mathbf{M}_{ij} is given by $\mathbf{M}_{ij} = \mathbf{M}_{ij}^t + \mathbf{M}_{ij}^r$, where $\mathbf{M}_{ij}^t = \Theta(\delta_{ij,n}) [d/2 - \delta_{ij,n}] \mathbf{e}_{ij,n} \times \mathbf{F}_{ij,t}^c$, and \mathbf{M}_{ij}^r is the torque associated with the rolling resistance at the contact point between particles i and j and is computed through the model (14, 17)

$$\mathbf{M}_{ij}^r(t + \Delta t) = \min \left(M_{ij}^{r,m}, |\mathbf{M}_{ij}^r(t) - k_r \boldsymbol{\omega}_{ij} \Delta t| \right) \frac{\mathbf{M}_{ij}^r(t) - k_r \boldsymbol{\omega}_{ij} \Delta t}{|\mathbf{M}_{ij}^r(t) - k_r \boldsymbol{\omega}_{ij} \Delta t|}, \quad [15]$$

where $M_{ij}^{r,m} = \mu_r R_{\text{eff}} |\mathbf{F}_{ij,n}^c|$, with μ_r standing for the coefficient of rolling resistance. Furthermore, $\boldsymbol{\omega}_{ij} = \boldsymbol{\omega}_i - \boldsymbol{\omega}_j$, Δt denotes the time step, and $k_r = k_t \sqrt{\delta_{ij,n}} R_{\text{eff}}^2$ (17, 51, 52). The magnitude of the spring torque \mathbf{M}_{ij}^r is, thus,

upper bounded by the full mobilization torque $\mu_r R_{\text{eff}} |F_{ij,n}^c|$, which means that rolling resistance behaves perfectly plastic beyond this upper bound.

Numerical Integration. The integration was performed using the open source Discrete Element Method particle simulation software LIGGGHTS (which stands for LAMMPS Improved for General Granular and Granular Heat Transfer Simulations) (52), along with the extensions introduced in ref. 15, to account for the computation of the dissipative term in the contact model (Eqs. 10 and 11), following ref. 44, and the attractive particle interaction force model (15, 47, 48) defined in Eq. 13. The integration time step Δt has been about 10% of the collision time T_{col} between two particles, defined from Hertz's elastic theory for the undamped, noncohesive situation; i.e., $T_{\text{col}} \approx 3.21(m_{\text{eff}}/k_n)^{2/5} \cdot v_{\text{imp}}^{-1/5}$ (12), where $m_{\text{eff}} = m/2$, and v_{imp} denotes the relative normal velocity of the particles at impact.

Model Parameters. The values of Young's modulus, Poisson's ratio, particle density, and surface energy density, listed in Table 1, are consistent with glass beads (15, 49), and we take the coefficients of sliding and rolling friction following calibration results from previous DEM simulations (6, 14–17, 46, 53, 54). The collisions of the particles with the frictional bottom wall are modeled using the same material parameters, while the wall is regarded as cohesionless and one of the collision partners has infinite mass and radius (15).

Furthermore, the normal damping coefficient A_n is computed based on the coefficient of restitution ε_{ref} associated with a reference collisional velocity v_{imp} , assuming only contact forces (no cohesion) (44). Based on previous calibration of the coefficient of restitution for use in DEM studies of the angle of repose (53, 54), here we adopt ε_{ref} in the range between 0.2 and 0.4, for $v_{\text{imp}} = 1.0$ m/s. All results presented in this article refer to $\varepsilon_{\text{ref}} = 0.2$, but we have found that using $\varepsilon_{\text{ref}} = 0.4$ still leads to a reasonable quantitative agreement between our numerical predictions for θ_r and the experimental data in Fig. 2. However, we reinforce that the main contribution of our article consists of a mathematical expression that is robust with respect to details of interparticle

interactions, encoded in the parameters $\mu_{\text{eff},\infty}$ and β . The role of various ingredients that have been neglected in our simulations, such as torsion (13) and long-range electrostatic interactions, should be elucidated in future work.

Numerical Experiments to Estimate the Packing Fraction, ϕ , as a Function of Particle Size and Gravity. Fig. 5 displays the results from numerical experiments to estimate the packing fraction ϕ as a function of d and g . Each of these experiments consists of releasing from rest a monodisperse packing of 20% initial volume fraction composed of 11,039 (initially noncontacting) particles randomly distributed over the simulation domain—a vertical rectangular box of horizontal dimensions $L_x \times L_y$, with $L_x = L_y = 17d$ and height $100d$. Boundary conditions are the same as in the experiments of the angle of repose, except that periodic boundary conditions are applied in the horizontal directions (15). Once the particles have settled due to the action of gravity, we compute the packing density of the granular column using $\phi = n_\phi \cdot (\pi/6) d^3 / [L_x \cdot L_y \cdot (H_U - H_I)]$, where n_ϕ is the number of particles with center-of-mass position between $H_I = 0.3z_{\text{max}}$ and $H_U = 0.7z_{\text{max}}$, with z_{max} denoting the center-of-mass position of the highest particle in the granular column (15). We find that ϕ differs negligibly over different realizations of the same experiment (each realization with different initial random positions of the particles). Therefore, each value of ϕ presented in Fig. 5 has been obtained based on one realization for the corresponding value of d and g , but by averaging over the four vertical subcolumns obtained by halving L_x and L_y (15), the associated SD corresponding to the error bars in Fig. 5 (i.e., the same protocol as in ref. 15 but including the effect of gravity in the investigation).

Data Availability. All study data are included in the main text.

ACKNOWLEDGMENTS. We thank Sandesh Kamath for assistance with the numerical interface between the DEM implementation of ref. 15 and the latest version of LIGGGHTS, Yaping Shao for discussions, and the German Research Foundation for funding through the Heisenberg Programme and Grant RI 2497/6-1.

- H. Chen, Y. L. Liu, X. Q. Zhao, Y. G. Xiao, Y. Liu, Numerical investigation on angle of repose and force network from granular pile in variable gravitational environments. *Powder Technol.* **283**, 607–617 (2015).
- A. C.-Y. Wong, Characterization of the flowability of glass beads by bulk densities ratio. *Chem. Eng. Sci.* **55**, 3855–3859 (2000).
- N. Pilpel, The flow properties of magnesia. *J. Pharm. Pharmacol.* **16**, 705–716 (1964).
- J. T. Carstensen, P.-C. Chan, Relation between particle size and repose angles of powders. *Powder Technol.* **15**, 129–131 (1976).
- Y. C. Zhou, B. H. Xu, A. B. Yu, P. Zulli, An experimental and numerical study of the angle of repose of coarse spheres. *Powder Technol.* **125**, 45–54 (2002).
- V. Hassanzadeh, C. M. Wensrich, R. Moreno-Atanasio, Elucidation of the role of cohesion in the macroscopic behaviour of coarse particulate systems using DEM. *Powder Technol.* **361**, 374–388 (2020).
- S. Ji, H. H. Shen, Contrasting terrestrial and lunar gravity: Angle of repose and incline flows. *Earth Space* **2006**, 1–8 (2006).
- M. W. Telfer et al., Dunes on Pluto. *Science* **360**, 992–997 (2018).
- C. B. Beddingfield et al., Landslides on Charon. *Icarus* **335**, 113383 (2020).
- P. A. Cundall, O. D. L. Strack, A discrete element model for granular assemblies. *Geotechnique* **29**, 47–65 (1979).
- N. V. Brilliantov, F. Spahn, J.-M. Hertzsch, T. Pöschel, Model for collisions in granular gases. *Phys. Rev. E Stat. Phys. Plasmas Fluids Relat. Interdiscip. Topics* **53**, 5382–5392 (1996).
- J. Schäfer, S. Dippel, D. E. Wolf, Force schemes in simulations of granular materials. *J. Phys. I France* **6**, 5–20 (1996).
- S. Luding, Cohesive, frictional powders: Contact models for tension. *Granul. Matter* **10**, 235 (2008).
- J. Ai, J. F. Chen, J. M. Rotter, J. Y. Ooi, Assessment of rolling resistance models in discrete element simulations. *Powder Technol.* **206**, 269–282 (2011).
- E. J. R. Parteli et al., Attractive particle interaction forces and packing density of fine glass powders. *Sci. Rep.* **4**, 6227 (2014).
- J. Schmidt et al., Packings of micron-sized spherical particles: Insights from bulk density determination, X-ray microtomography and discrete element simulations. *Adv. Powder Technol.* **31**, 2293–2304 (2020).
- C. M. Wensrich, A. Katterfeld, Rolling friction as a technique for modelling particle shape in DEM. *Powder Technol.* **217**, 409–417 (2012).
- G. Lumay et al., Measuring the flowing properties of powders and grains. *Powder Technol.* **224**, 19–27 (2012).
- Y. Li, Y. Xu, C. Thornton, A comparison of discrete element simulations and experiments for 'sandpiles' composed of spherical particles. *Powder Technol.* **160**, 219–228 (2005).
- Y. Matsukara, H. Obanawa, Effect of grain diameter and packing condition on the avalanching depth on a slope composed of dry granular materials. *Tsukuba Geoenvironmental Sciences* **1**, 19–25 (2005).
- E. M. Culligan, H. K. Christenson, Cohesion of granular matter in subzero humidity. *J. Phys. Chem. C* **118**, 15929–15933 (2014).
- J. H. Choi, E. T. Kang, J. W. Lee, U. S. Kim, W. S. Cho, Materials and process development for manufacturing porcelain figure using a binder jetting 3D printer. *J. Ceram. Process. Res.* **19**, 43–49 (2018).
- J. R. Metcalf, Angle of repose and internal friction. *Int. J. Rock Mech. Min. Sci.* **3**, 155–161 (1966).
- A. Anand, J. S. Curtis, C. R. Wassgren, B. C. Hancock, W. R. Ketterhagen, Segregation of cohesive granular materials during discharge from a rectangular hopper. *Granul. Matter* **12**, 193–200 (2010).
- A. Gans, O. Pouliquen, M. Nicolas, Cohesion-controlled granular material. *Phys. Rev. E* **101**, 032904 (2020).
- C. Lanzerstorfer, Dusts from dry off-gas cleaning: Comparison of flowability determined by angle of repose and with shear cells. *Granul. Matter* **19**, 58 (2017).
- C. Song, P. Wang, H. A. Makse, A phase diagram for jammed matter. *Nature* **453**, 629–632 (2008).
- P. G. Hofmeister, J. Blum, D. Heisselmann, The flow of granular matter under reduced gravity conditions. *AIP Conf. Proc.* **1145**, 71–74 (2009).
- P. G. Hofmeister, J. Blum, D. Heisselmann, Flows of dense granular media. *Annu. Rev. Fluid Mech.* **40**, 1–24 (2008).
- M. G. Kleinhans, H. Markies, S. J. de Vet, A. C. in 't Veld, F. N. Postema, Static and dynamic angles of repose in loose granular materials under reduced gravity. *J. Geophys. Res.* **116**, E11004 (2011).
- C. M. Dury, G. H. Ristow, J. L. Moss, M. Nakagawa, Boundary effects on the angle of repose in rotating cylinders. *Phys. Rev. E* **57**, 4491–4497 (1998).
- B. R. White, S. P. Klein, Dynamic shear of granular material under variable gravity conditions. *Am. Inst. Aeronaut. J.* **28**, 1701–1702 (1990).
- O. R. Walton, C. Pamela de Moor, K. S. Gill, Effects of gravity on cohesive behavior of fine powders: Implications for processing Lunar regolith. *Granul. Matter* **9**, 353–363 (2007).
- A. Brucks, T. Arndt, J. M. Ottino, R. M. Lueptow, Behavior of flowing granular materials under variable g. *Phys. Rev. E Stat. Nonlin. Soft Matter Phys.* **75**, 032301 (2007).
- V. Schatz, H. Tsoar, K. S. Edgett, E. J. R. Parteli, H. J. Herrmann, Evidence for indurated sand dunes in the Martian north polar region. *J. Geophys. Res.* **111**, E04006 (2006).
- H. Nakashima et al., Determining the angle of repose of sand under low-gravity conditions using discrete element method. *J. Terramechs.* **48**, 17–26 (2011).
- C. Atwood-Stone, A. S. McEwen, Avalanche slope angles in low-gravity environments from active Martian sand dunes. *Geophys. Res. Lett.* **40**, 2929–2934 (2013).
- D. Geldart, E. C. Abdullah, A. Hassanpour, L. C. Nwoke, I. Wouters, Characterization of powder flowability using measurement of angle of repose. *China Particology* **4**, 104–107 (2006).
- X. L. Deng, R. N. Davé, Dynamic simulation of particle packing influenced by size, aspect ratio and surface energy. *Granul. Matter* **15**, 401–415 (2013).

40. R. P. Behringer, B. Chakraborty, The physics of jamming for granular materials: A review. *Rep. Prog. Phys.* **82**, 012601 (2019).
41. L. E. Silbert et al., Granular flow down an inclined plane: Bagnold scaling and rheology. *Phys. Rev. E Stat. Nonlin. Soft Matter Phys.* **64**, 051302 (2001).
42. R. Ramirez, T. Pöschel, N. V. Brilliantov, T. Schwager, Coefficient of restitution of colliding viscoelastic spheres. *Phys. Rev. E Stat. Phys. Plasmas Fluids Relat. Interdiscip. Topics* **60**, 4465–4472 (1999).
43. T. Schwager, T. Pöschel, Coefficient of restitution for viscoelastic spheres: The effect of delayed recovery. *Phys. Rev. E Stat. Nonlin. Soft Matter Phys.* **78**, 051304 (2008).
44. P. Müller, T. Pöschel, Collision of viscoelastic spheres: Compact expressions for the coefficient of normal restitution. *Phys. Rev. E Stat. Nonlin. Soft Matter Phys.* **84**, 021302 (2011).
45. T. Schwager, V. Becker, T. Pöschel, Coefficient of tangential restitution for viscoelastic spheres. *Eur. Phys. J. E Soft Matter* **27**, 107–114 (2008).
46. C. H. Rycroft, A. V. Orpe, A. Kudrolli, Physical test of a particle simulation model in a sheared granular system. *Phys. Rev. E Stat. Nonlin. Soft Matter Phys.* **80**, 031305 (2009).
47. H. C. Hamaker, The London-van der Waals attraction between spherical particles. *Physica* **4**, 1058–1072 (1937).
48. M. L. Eggersdorfer, D. Kadau, H. J. Herrmann, S. E. Pratsinis, Fragmentation and restructuring of soft-agglomerates under shear. *J. Colloid Interface Sci.* **342**, 261–268 (2010).
49. M. Götzinger, W. Peukert, Dispersive forces of particle-surface interactions: Direct AFM measurements and modelling. *Powder Technol.* **130**, 102–109 (2003).
50. J. Israelachvili, *Intermolecular & Surface Forces* (Academic Press, London, UK, 1998).
51. K. Iwashita, M. Oda, Rolling resistance at contacts in simulation of shear band development by DEM. *J. Eng. Mech.* **124**, 285–292 (1998).
52. C. Kloss, C. Goniva, A. Hager, S. Amberger, S. Pirker, Models, algorithms and validation for opensource DEM and CFD-DEM. *Prog. Comput. Fluid Dyn.* **12**, 140–152 (2012).
53. P. Frankowski, M. Morgeneyer, Calibration and validation of DEM rolling and sliding friction coefficients in angle of repose and shear measurements. *AIP Conf. Proc.* **1542**, 851 (2013).
54. R. Poisel, A. Preh, “Modifications of PFC^{3D} for rock mass fall modeling” in *Continuum and Distinct Element Numerical Modeling in Geo-Engineering*, R. Hart, C. Detournay, P. Cundall, Eds. (Itasca Consulting Group, Inc., Minneapolis, MN, 2008), pp. 29–38.